

OPTIMIZING THE ENERGY AND THE SPECTRAL EFFICIENCY OF 5G TELECOMMUNICATION NETWORK

RAFALINIRINA Haingomalala Sandra¹, RANDRIAMITANTSOA Paul Auguste²

¹ PhD student, TASI, ED-STII, Antananarivo, Madagascar

² Thesis director, TASI, ED-STII, Antananarivo, Madagascar

ABSTRACT

The energy consumption of the communications technology industry and related energy-related pollution are becoming major societal and economic concerns. This has spurred academic and industry activity in the new field of green cellular research, recently spurred by the SMART 2020 report and the Green Touch consortium. The ultimate goal is to design new architectures and innovative networking technologies needed to meet the explosive growth of cellular data demand without increasing power consumption. In this article, we focus on optimizing the performance of 5G telecommunications networks through MIMO and millimeter wave techniques.

Keywords : 5G, Energy Efficiency, Spectral Efficiency, Massive MIMO, Millimeter wave

1. INTRODUCTION

The market demands that the capacity of 5G networks be higher than that of these predecessors. By using a large number of antennas, Massive MIMO can significantly improve spectral efficiency by making extensive use of available space resources. Migration to higher frequencies could release a large amount of available bandwidth to support broadband transmission. In particular, the millimeter wave may be the promising candidate. Thus lies the need to study the operation of Massive MIMO systems in certain frequency domains. In this article, we will highlight methods for optimizing Energy Efficiency and Spectrum Efficiency to ensure performance requirements for 5G telecommunications networks. Firstly, communication scenarios between the base station and the user equipment in the 700 MHz bands will be addressed in order to make the ideal choice of the number of antennas M at the base station, the number K of active user equipment and the power of emission ρ so as to uniformly cover a dense urban space and a large building with Optimum Energy Efficiency for the system. An alternative optimization algorithm is used to find the optimal values M , K and ρ in a ZF linear processing system. This algorithm maximizes Energy Efficiency by optimizing M , K and ρ separately when the other two are fixed. The global optimum can be obtained by an exhaustive search on all the pair combinations (K, M) and calculation of the optimal distribution of the power. A Monte Carlo method based on power allocation and a power consumption model will be used for a system using MRT / MRC linear processing. The values of K and M will therefore be used to calculate the optimum overall Energy Efficiency values achievable for ZF and MRT / MRC linear processing systems. Using these parameters maximizing the Energy Efficiency, one will also find results of traffic capacity, total power of emission and power radiated by the antennas. Secondly, in the case of communication between base station and user equipment, the research object will highlight the millimeter wave systems. The work will compare different precoding methods, namely beamforming-based analog precodings, hybrid precodings based on Spatially Sparse algorithm, and the Successive Interference Cancellation algorithm. Spectral Efficiency and Energy Efficiency will be our main performance metrics for this second optimization work.

2. 5G telecommunication network

2.1 Global Architecture

The overall architecture of the 5G telecommunications network consists of a Radio Access or Next Generation RAN (NG-RAN) and a core network or 5G Core (5GC) [1] [2]. Figure 1 illustrates this architecture.

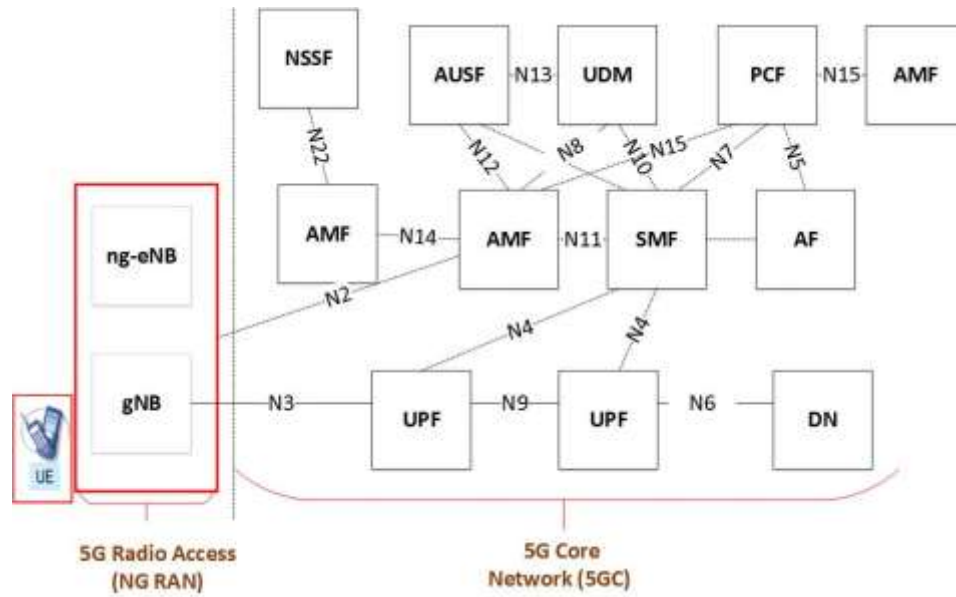


Fig - 1 : 5G architecture and interfaces between entities

User Equipment (UE) communicate with the base stations either by a 5G radio link or by a 4G radio link. If the communication is in 5G, the base station is named next Generation Node Base Station (gNB), if the communication is in 4G, the base station is an evolved 4G eNB base station to interconnect with the 5G core network. The base station is Next Generation -eNb (ng-eNb) or eLTE-eNB. Our field of study is at the level of red blocks shown in Figure 1.

2.2 Block diagram of the base station

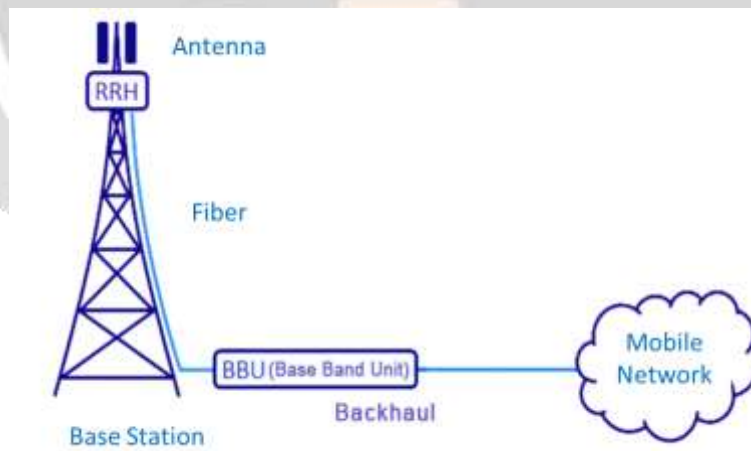


Fig - 2 : Base Station Architecture

A radio base station illustrated in Figure 2 may be functionally [3] [4] separated into:

- BBU = baseband unit (sometimes referred to as a digital unit), which generates and processes a scanned baseband RF signal
- RRH = Remote Radio Head that creates the analog RF transmission signal from the baseband signal and transmits it to the antenna, scans the receive signal

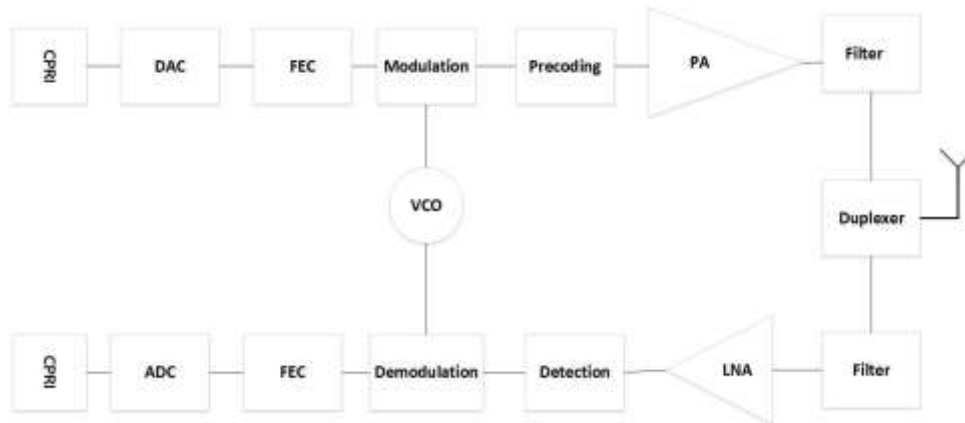


Fig -3 : Block Diagram of RRH

3. Optimization of Energy Efficiency

Energy efficiency is the ratio of the useful energy produced by a system to the total energy consumed to make it

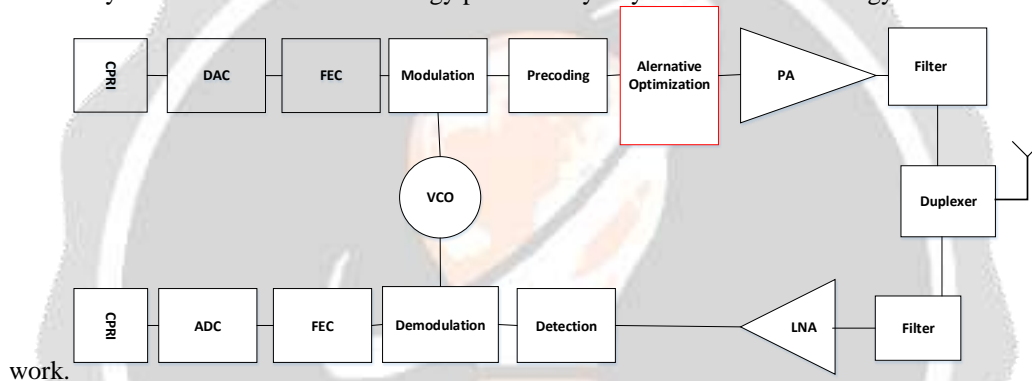


Fig -4 : Synoptic scheme RRH with EE optimization

In contrast to Figure 3, an alternative optimization block is shown in Figure 4 before the power amplifier block to ensure Energy Efficiency maximization for the multi-user MIMO system.

3.1. Modeling MU-MIMO systems

The MU-MIMO system or multi-user MIMO system is a multi-user system using MIMO technology. The base station is equipped with M antennas and can serve up to K users such as $M \gg K$. The system operates in TDD or Time-Division Duplexing mode using uplink and downlink linear processing.

3.1.1 TDD protocol

The TDD transmission protocol is a technique enabling a telecommunication channel, using the same transmission resource, to multiplex time transmission and reception.

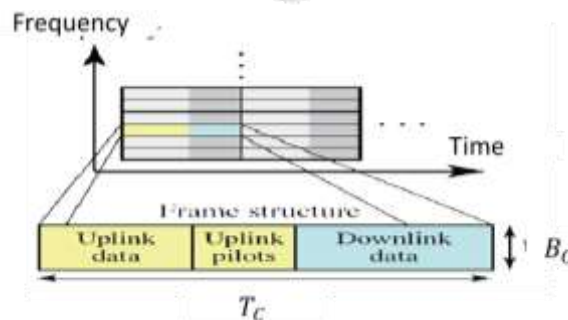


Fig -5 : Basic protocol for transmission in TDD mode

The bandwidth B_C is selected so that it is smaller than or equal to that provided for the bandwidth of coherence between the users. While T_C is smaller or equal to the coherence time of the anticipated user channels. The number of transmission symbols that fit within a coherence interval is given by the formula $U = B_C T_C$, referring to the Nyquist-Shannon sampling theorem. The transmission fraction is a fraction specified for an uplink transmission noted $\zeta^{(ul)}$ or downlink transmission noted $\zeta^{(dl)}$ so that the sum $\zeta^{(ul)} + \zeta^{(dl)} = 1$. As shown in Figure 6, uplink transmission takes place first with $U\zeta^{(ul)}$ symbols. The subsequent downlink of the transmission is represented by $U\zeta^{(dl)}$ symbols.

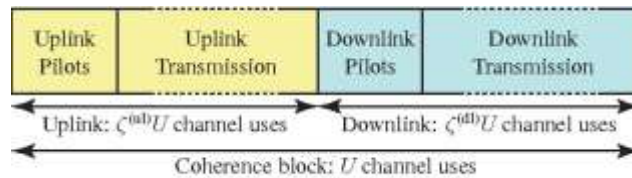


Fig -6: Protocole TDD

The signaling driver for the uplink occupies $\tau^{(ul)}K$ symbols and $\tau^{(dl)}K$ for the downlink. With this, it is noticed that $\tau^{(ul)}, \tau^{(dl)} \geq 1$ in order to activate the orthogonal pilot sequences among the UEs [5], [6], [7].

The uplink drivers allow the base station to estimate the UE channels.

Downlink drivers let each UE evaluate its actual channel and its variant interferences with the current precoding.

3.1.2 User Location Modeling

The distribution density function of users is defined by:

$$f(x) = \begin{cases} \frac{1}{\pi(d_{max}^2 - d_{min}^2)} & d_{min} \leq \|x\| \leq d_{max} \\ 0 & \text{autres} \end{cases} \quad (1)$$

Users are evenly distributed in a circular cell of maximum radius d_{max} . Note d_{min} the minimum distance of a user's location from the base station.

3.1.3 Channel fading model

The system is under the effect of large scale fading or fading phenomena due to path loss, dispersion and shading at the user's location x_k of a user k . The average attenuation at a reference distance d_0 is equal to $\overline{PL}(d_0)$, the average attenuation is given by:

$$\overline{PL}(d) = \overline{PL}(d_0) \left(\frac{d}{d_0}\right)^k \quad (2)$$

With k the exponent of path loss. In decibel, the attenuation is:

$$\overline{PL}(d)_{dB} = \overline{PL}(d_0)_{dB} + 10k \log\left(\frac{d}{d_0}\right) \quad (3)$$

3.1.3.1 Path loss modeling in a dense urban space

In a dense urban environment, the value of the exponent k varies from 2 to 5. We have the modeling of the propagation loss as follows:

$$\overline{PL}(d) = \overline{PL}(d_0) \left(\frac{d}{d_0}\right)^k \text{ pour } 2 < k < 5 \quad (4)$$

3.1.3.2 Path loss modeling in a building

Taking the case of a system inside a large building, the value of the exponent k will be 1.6. We have the modeling of the propagation loss as follows:

$$\overline{PL}(d) = \overline{PL}(d_0) \left(\frac{d}{d_0}\right)^{1.6} \quad (5)$$

In these two cases of path loss exhibiting loss of path seen previously, let's $\overline{PL}(d) = l(x)$, $\left(\frac{d}{d_0}\right) = \frac{1}{\|x\|^k}$, $\overline{PL}(d_0) = \bar{d}$

Large-scale fading can be generally presented by the $l(\cdot): \mathbb{R}^2 \rightarrow \mathbb{R}$ function and will therefore be:

$$l(x) = \frac{\bar{d}}{\|x\|^k} \quad (6)$$

Note that $\bar{d} > 0$ regulates channel attenuation at distance d_{min} and $d_{min} \leq \|x\| \leq d_{max}$

The average inverse attenuation of the channel plays a key role in all subsequent discussions.

The average channel inverse attenuation is defined by:

$$\mathbb{E}_x \left\{ (l(x))^{-1} \right\} = \frac{d_{max}^{k+2} - d_{min}^{k+2}}{\bar{d} \left(1 + \frac{k}{2}\right) (d_{max}^2 - d_{min}^2)} \quad (7)$$

3.1.4 Channel model and linear processing

The M antennas at the base station are sufficiently spaced apart that the channel components between the base station antennas and the single antenna user equipment are not correlated.

3.1.4.1 Channel model

The channel model is characterized by the channel vector $h_k = [h_{k,1}, h_{k,2}, \dots, h_{k,M}]^T \in \mathbb{C}^{M \times 1}$ having inputs $\{h_{k,n}\}$ describing the instantaneous propagation channel between the n^{th} base station antenna and the k^{th} UE. We assume a small scale fading Rayleigh distribution such as $h_k \sim \mathcal{CN}(0_M, l(x_k) I_M)$, which is a valid model for large and small networks.

3.1.4.2 Linear Processing

Let $G = [g_1, g_2, \dots, g_K] \in \mathbb{C}^{M \times K}$ be the linear combination matrix in reception for the uplink. Column g_k is assigned to k^{th} UE. The linear treatments MRC and ZF are considered for uplink detection, which gives:

$$G = \begin{Bmatrix} H & \text{MRC} \\ H(HH^H)^{-1} & \text{ZF} \end{Bmatrix} \quad (8)$$

where $H = [h_1, h_2, \dots, h_K]$ contains all user channels.

Similarly, we consider the MRT and ZF precodings for the downlink. Noting by $V = [v_1, v_2, \dots, v_K] \in \mathbb{C}^{M \times K}$ the precoding matrix, we have this:

$$V = \begin{Bmatrix} H & \text{MRT} \\ H(HH^H)^{-1} & \text{ZF} \end{Bmatrix} \quad (9)$$

It is natural to define $V = G$ to reduce computational complexity.

Although conventional systems have a great disparity between peak and average flow rates, we aim to design the system to ensure a uniform raw flow rate \bar{R} (in bits / second) for any active UE, of which $\zeta^{(ul)}\bar{R}$ is the flow rate uplink and $\zeta^{(dl)}\bar{R}$ is the downlink. This is achieved by combining the linear processing with an appropriate power allocation.

According to Gaussian code book assumptions, linear processing and perfect CSI, the uplink rate (in bit / second) of the k^{th} UE is expressed as follows:

$$R_k^{(ul)} = \zeta^{(ul)} \left(1 - \frac{\tau^{(ul)}K}{U\zeta^{(ul)}} \right) \bar{R}_k^{(ul)} \quad (10)$$

where the factor $\left(1 - \frac{\tau^{(ul)}K}{U\zeta^{(ul)}} \right)$ represents the pilot overhead the uplink transmission fraction.

A functional diagram of the rising transmission with linear detection is provided in the figure below.

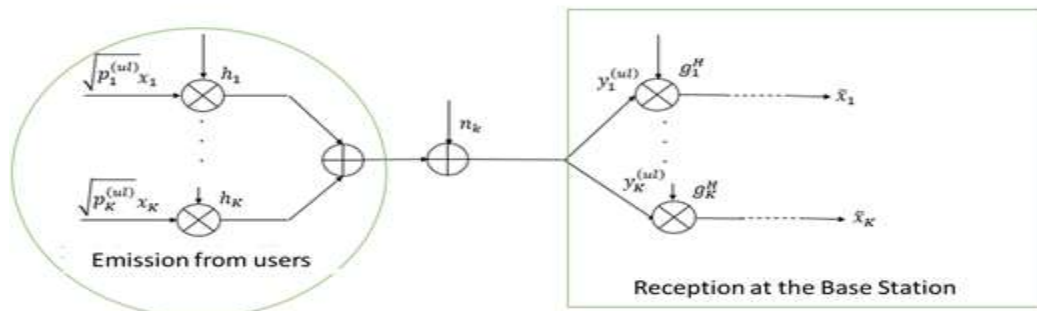


Fig -7 : Block diagram of an uplink transmission with linear detection in a single-cell MIMO multi-user network

Where x_k is the normalized transmission symbol (with $E\{|x_k|^2\} = 1$) and $p_k^{(ul)}$ the transmission power of the user k in the cell. The receiver equipment at the base station is contaminated with additive white noise, modeled by the vector $n_k \in \mathbb{C}^M$ following a Gaussian distribution with circular symmetry of zero mean with a variance σ^2 , hence $n_k \sim \mathcal{CN}(0, \sigma^2 I_M)$. h_k is the user channel for the k^{th} user, g_k^H is the linear detection vector for the k^{th} user at the base station and the detected signal \tilde{x}_k corresponding to the user k for $k = 1, 2, \dots, K$.

In addition, the uplink raw bit rate (in bit / second) from the k^{th} UE, where "gross" refers to overhead factors that are not included, is expressed by:

$$\bar{R}_k^{(ul)} = \text{Blog}_2 \left(1 + \frac{p_k^{(ul)} |g_k^H h_k|^2}{\sum_{i=1, i \neq k}^K p_i^{(ul)} |g_k^H h_i|^2 + \sigma^2 \|g_k\|^2} \right) \quad (11)$$

A block diagram of downlink transmission is provided in Figure 8.

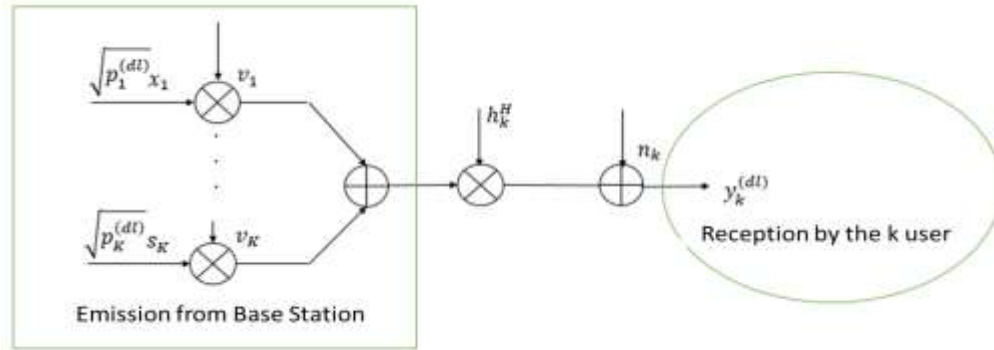


Fig -8 : Block diagram of downlink transmission with linear precoding for a MIMO system in a cell

Assuming perfect Gaussian and CSI directories, the downlink rate that can be achieved (in bit / second) of the k^{th} UE with linear processing is:

$$R_k^{(dl)} = \zeta^{(dl)} \left(1 - \frac{\tau^{(dl)} K}{U \zeta^{(dl)}} \right) \bar{R}_k^{(dl)} \quad (12)$$

where $\left(1 - \frac{\tau^{(dl)} K}{U \zeta^{(dl)}} \right)$ is the driver overhead on the downlink and $\bar{R}_k^{(dl)}$ is the raw bit rate (in bit / second) given by:

$$\bar{R}_k^{(dl)} = \text{Blog}_2 \left(1 + \frac{p_k^{(dl)} \frac{|h_k^H v_k|^2}{\|v_k\|^2}}{\left(\sum_{i=1, i \neq k}^K p_i^{(dl)} \frac{|h_k^H v_i|^2}{\|v_i\|^2} + \sigma^2 \right)} \right) \quad (13)$$

3.1.5 Energy Efficiency Optimization Problem Formulation

The total uplink and downlink EE is expressed by:

$$EE = \frac{\sum_{k=1}^K \left(\mathbb{E} \{ R_k^{(ul)} \} + \mathbb{E} \{ R_k^{(dl)} \} \right)}{P_{TX}^{(ul)} + P_{TX}^{(dl)} + P_{CP}} \quad (14)$$

Where $P_{TX}^{(ul)}$ and $P_{TX}^{(dl)}$ powers of the power amplifiers at the base station and UE respectively. P_{CP} is the total circuit consumption [8].

3.1.6 Optimization of the Energy Efficiency of MU-MIMO system in a dense urban space

3.1.6.1 EE optimization results in ZF and MRT / MRC treatment in dense urban space

The deployment model obtained in Figure 9 shows the set of achievable EE values with CSI perfect for ZF processing with different values of M up to 220 and K up to 150 [8].

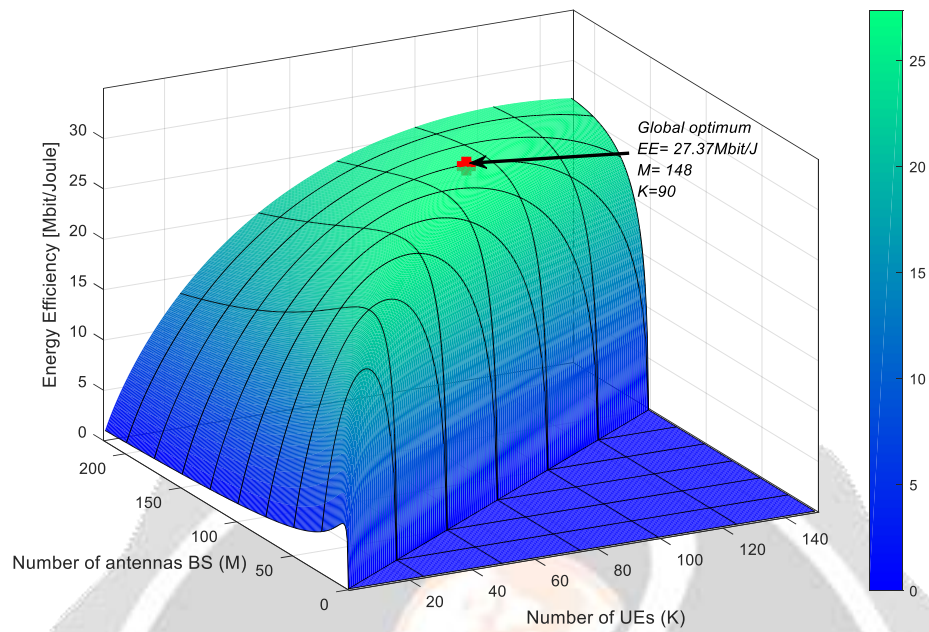


Fig -9 : Global Optimum in ZF at perfect CSI in dense urban space

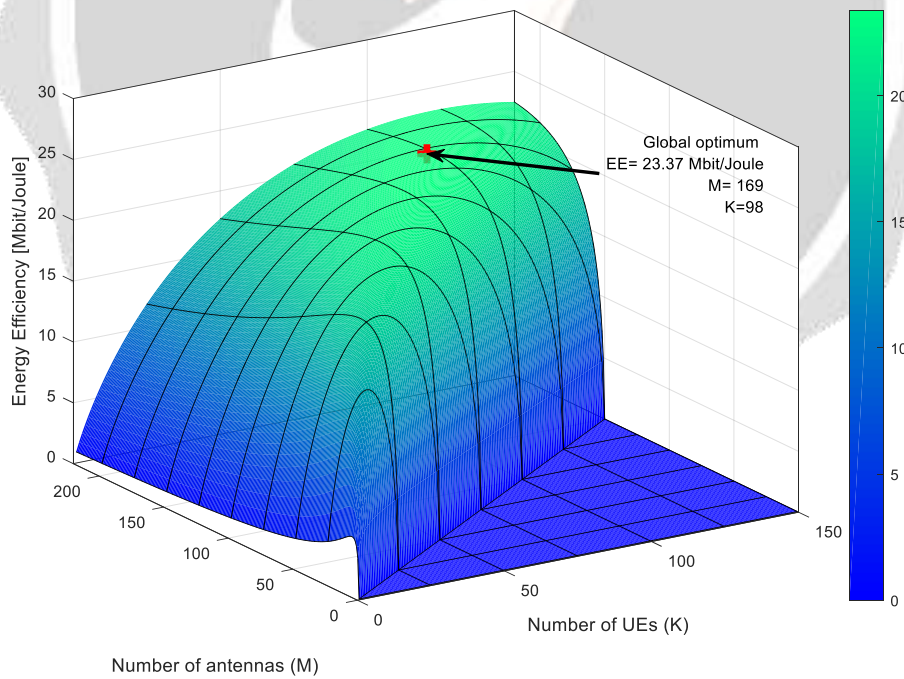


Fig -10 : Global optimum in ZF treatment at imperfect CSI in dense urban space

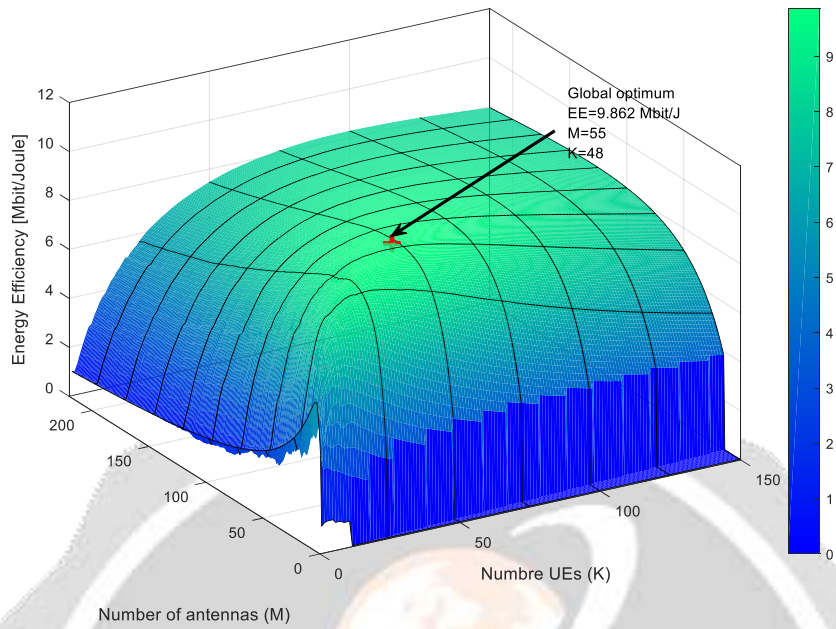


Fig -11 : Global optimum in MRT / MRC processing at perfect CSI in dense urban space

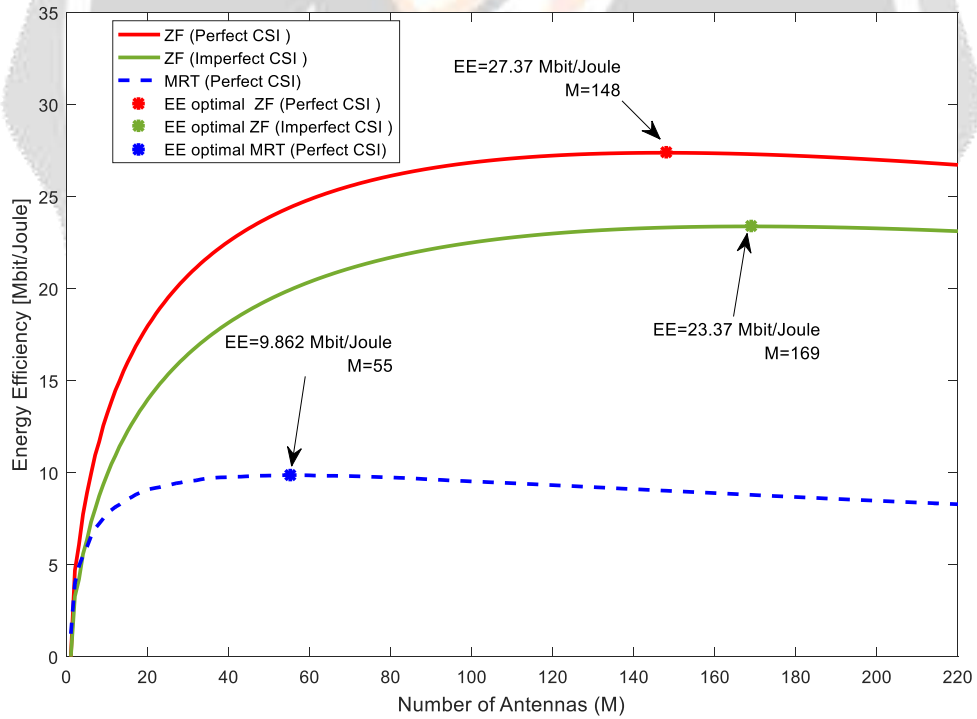


Fig -12 : Maximum EE values in the M range for optimal K values for each treatment in dense urban space

3.1.6.2 Total power results of power amplifier in urban space

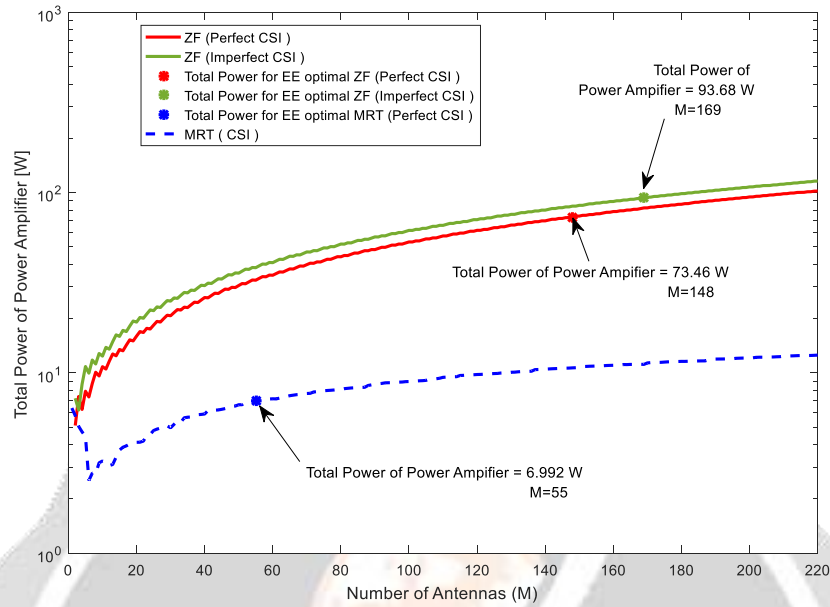


Fig -13 : Total energy consumption by power amplifier in dense urban space

3.1.6.3 Radiated Power Results by each antenna at the base station in dense urban space

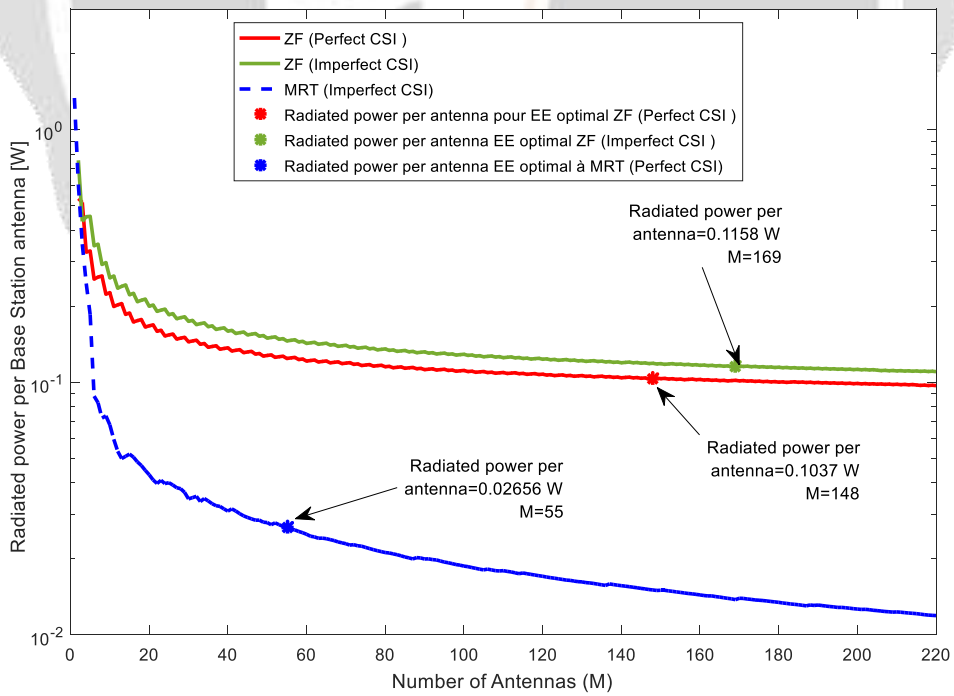


Fig -14 : Power radiated by each antenna at the base station

3.1.6.4 Results Area Traffic capacity in the urban environment

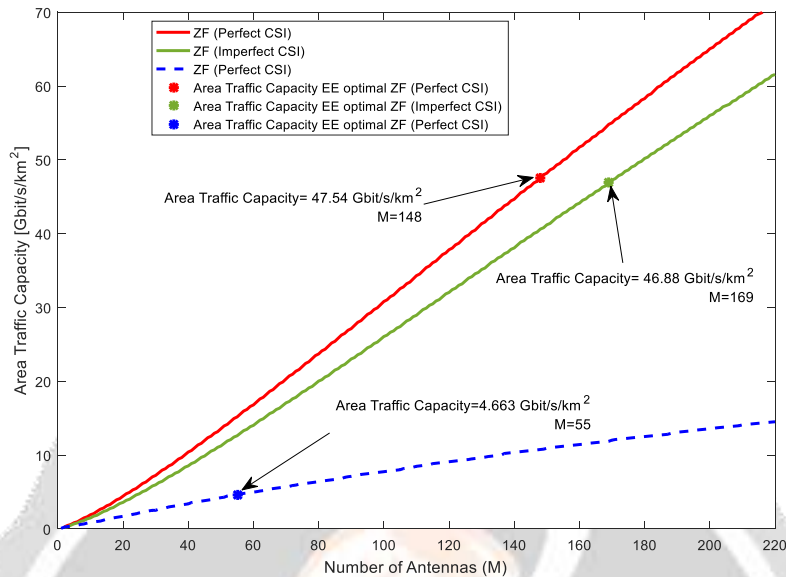


Fig -15 : Area Traffic capacity in dense urban space

3.1.7 Optimization of the Energy Efficiency of MU-MIMO system in a building

Either a system where the communication environment is inside a building with a surface $S = \pi D^2$ with $D = 50 m$. The signal propagation loss modeling differs from that used in the dense urban environment. We will therefore have a large-scale fading with a path loss path exhibitor equal to 1.6.

3.1.7.1 EE optimization results in ZF and MRT / MRC treatment in a building

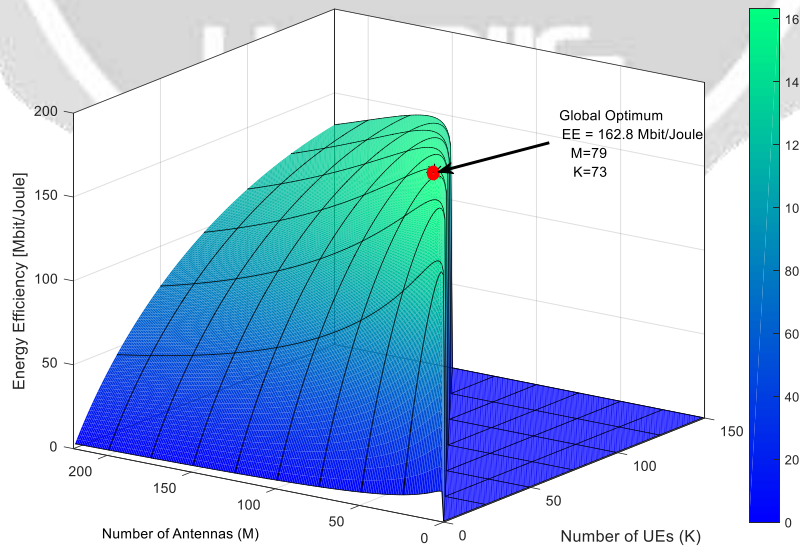


Fig -16 : Optimum global ZF treatment at CSI perfect in a building

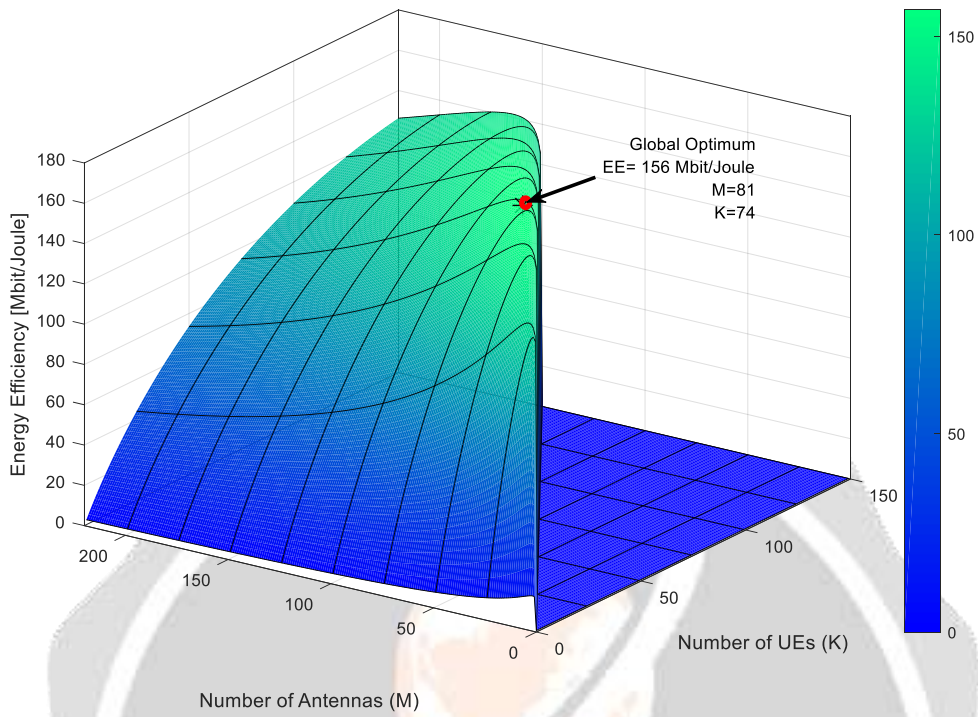


Fig -17 : Global optimum in ZF processing at imperfect CSI in a building

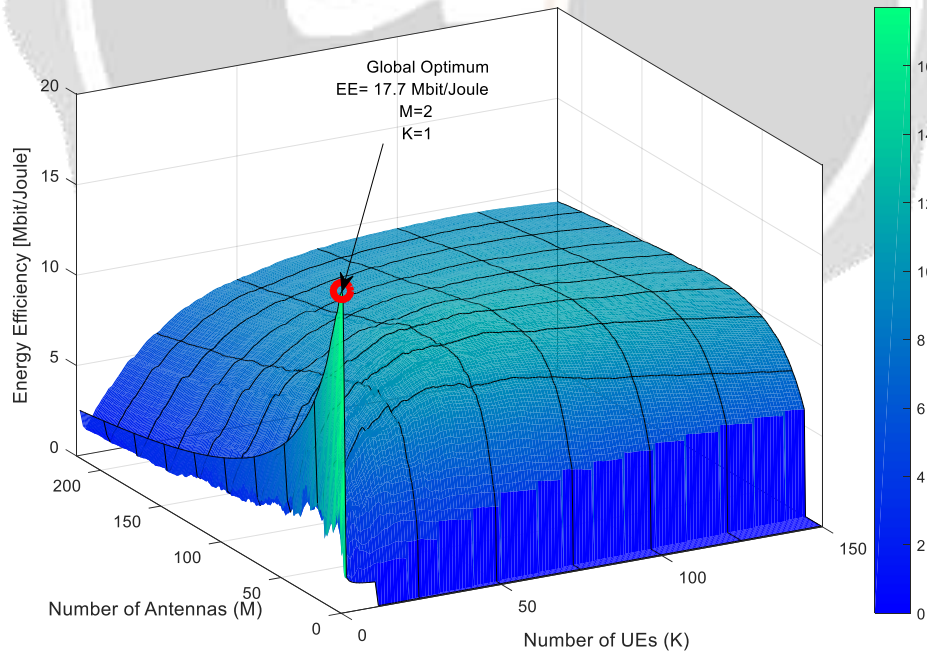


Fig -18 : Global Optimum in MRT / MRC at perfect CSI in a building

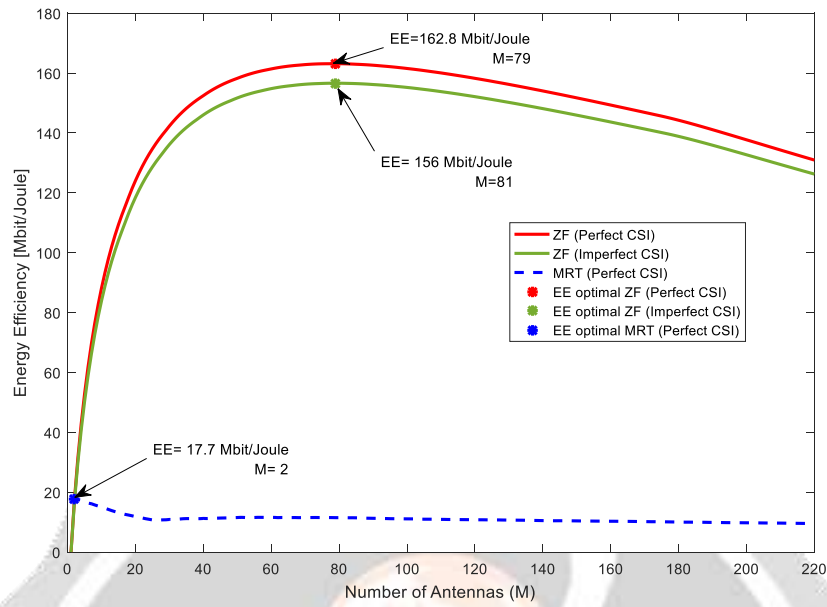


Fig-19 : Maximum values of EE for ZF at perfect CSI, ZF at imperfect CSI and MRT at CSI perfect for every treatment in a building

3.1.7.2 Total power PA results in a building

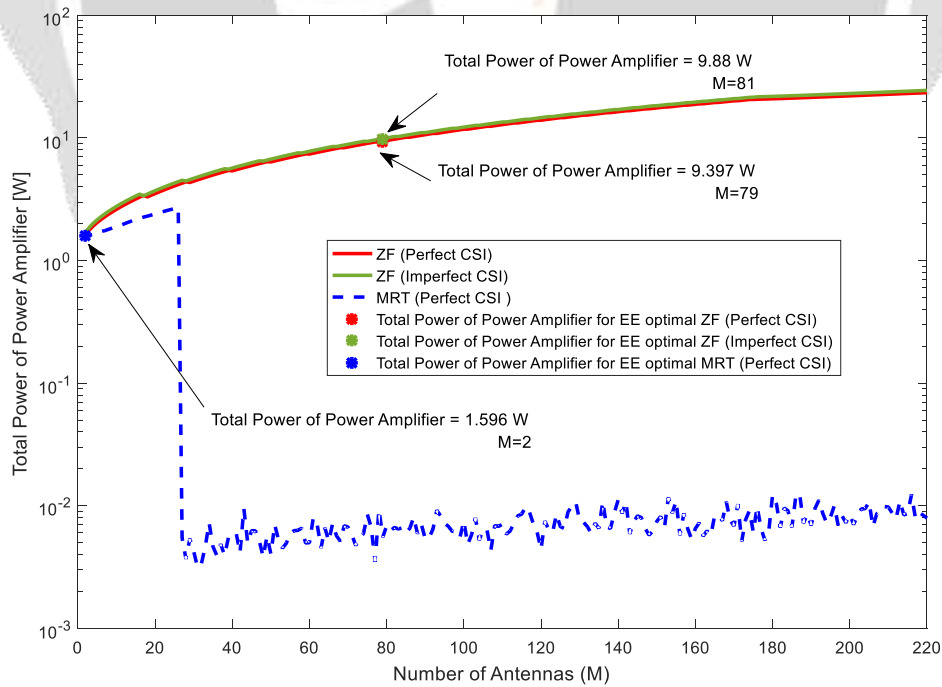


Fig -20 : Total power of power amplifiers in a building

3.1.7.3 Radiated Power results by each antenna at the base station

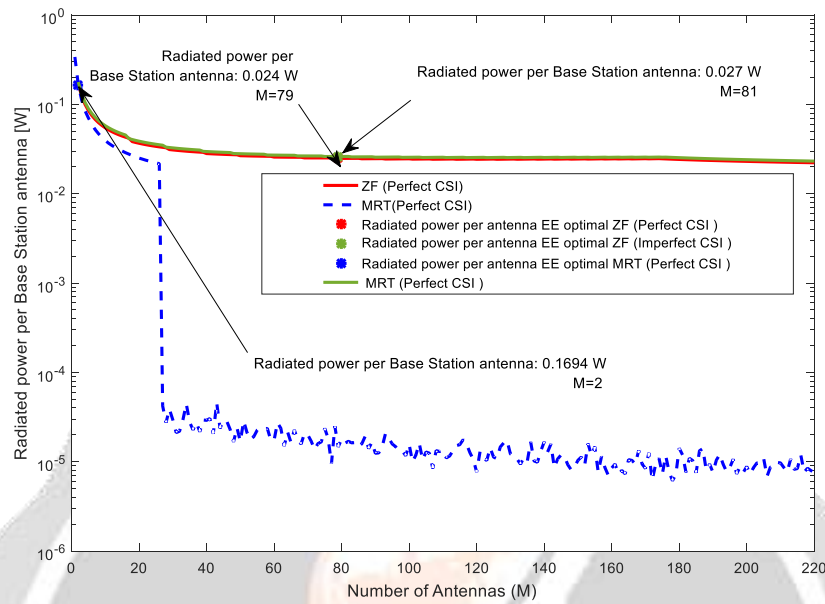


Fig -21 : Radiated Power by each antenna at the base station of the building

3.1.7.4 Results Area Traffic capacity in a building

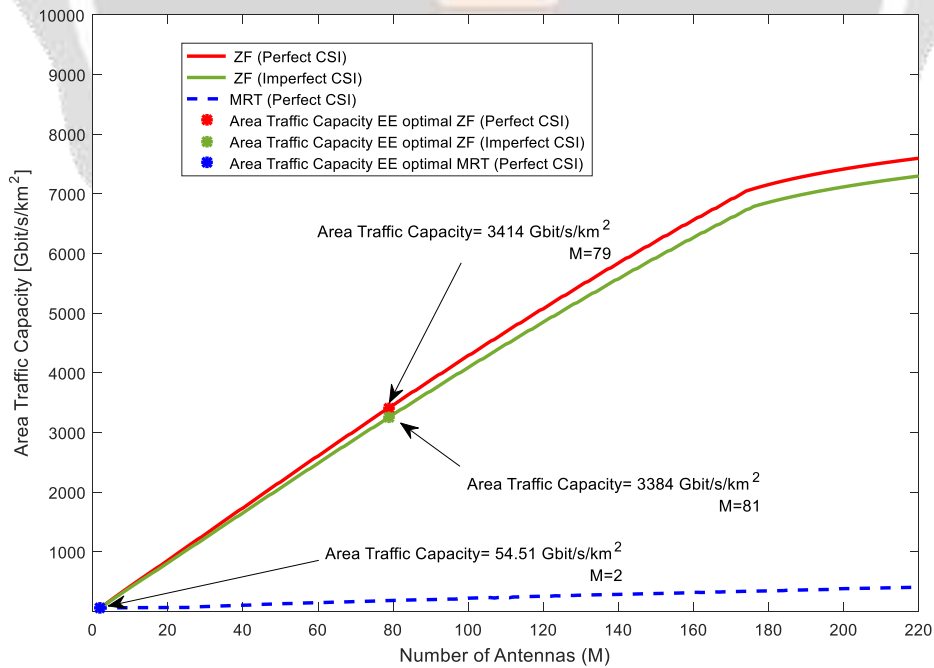


Fig -22 : Area Traffic capacity in a building

3.1.8 Energy Efficiency Optimization of Multicellular MU -MIMO System in a Dense Urban Environment and Large Infrastructure

A symmetric multicellular scenario is shown in Figure 23 for the simulation. The middle cell will be our field of study. The UE therein are placed in a uniform distribution. For this case, we will only consider interference from the two nearest cells. We will take a scenario for system at ZF. In Figure 23, the cells are divided into four clusters. Three different models of pilot reuse factor will be considered: the same drivers in all cells ($\tau^{(ui)} = 1$); two orthogonal sets of ($\tau^{(ui)} = 2$) drivers in cluster 1 and cluster 4; all groups have different orthogonal drivers ($\tau^{(ui)} = 4$) [8].

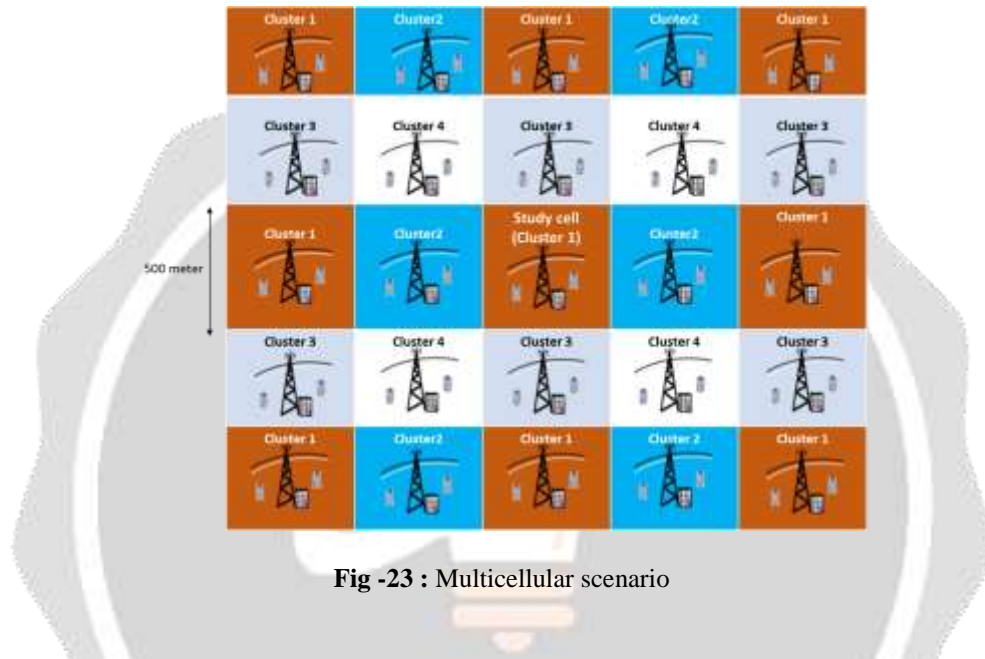


Fig -23 : Multicellular scenario

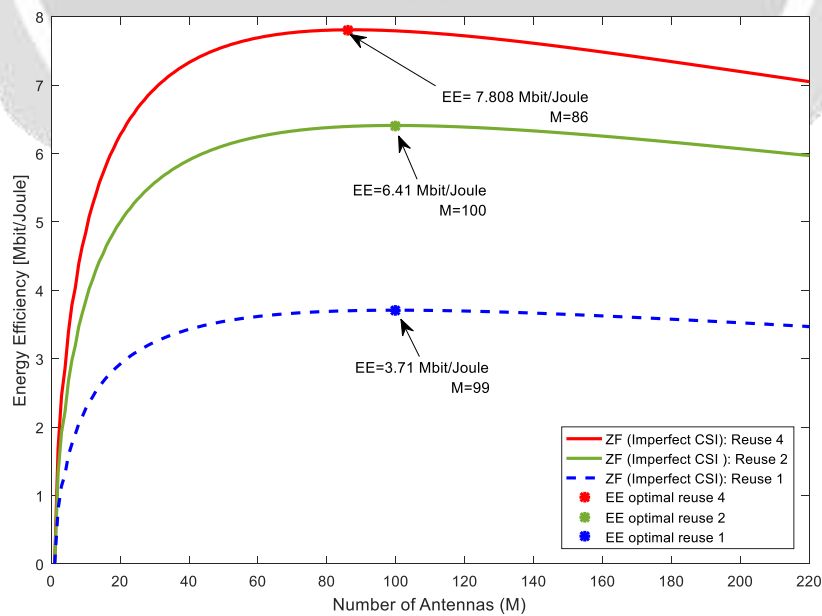


Fig-24 : EE maximum with pilot reuse 1,2, and 4, in dense urban space

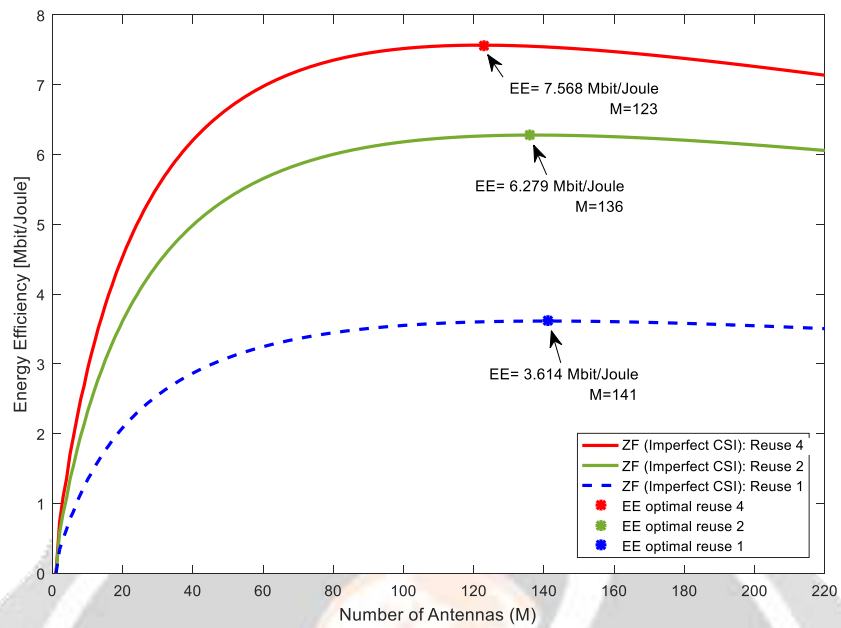


Fig -25 : EE maximum with pilot reuse 1,2, and 4, in a large infrastructure

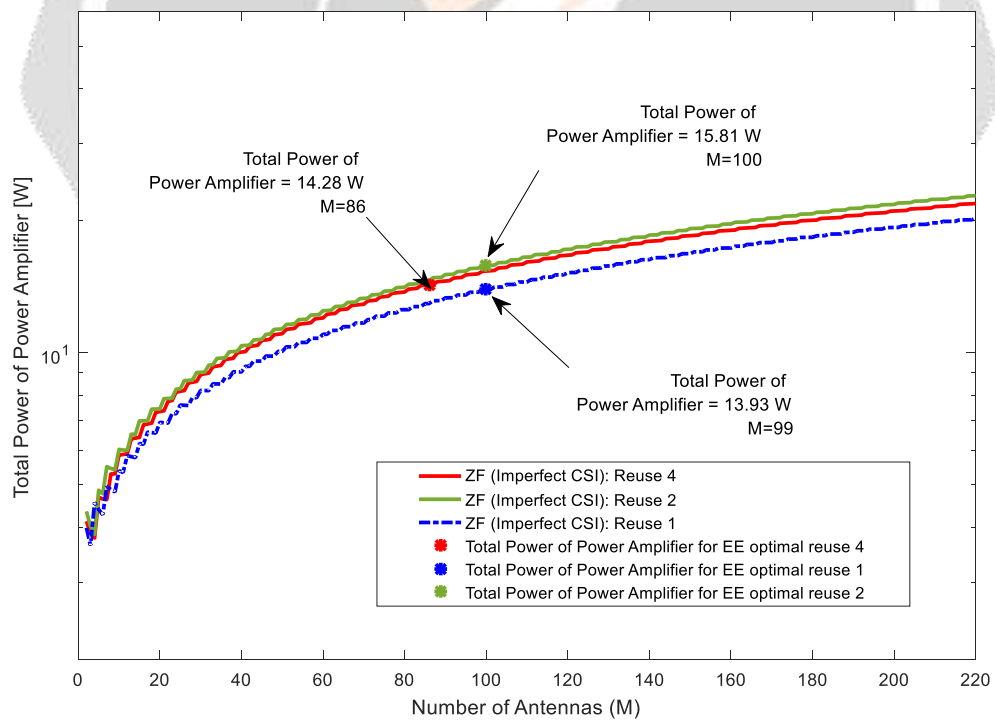


Fig -26 : Total powers PA in dense urban space

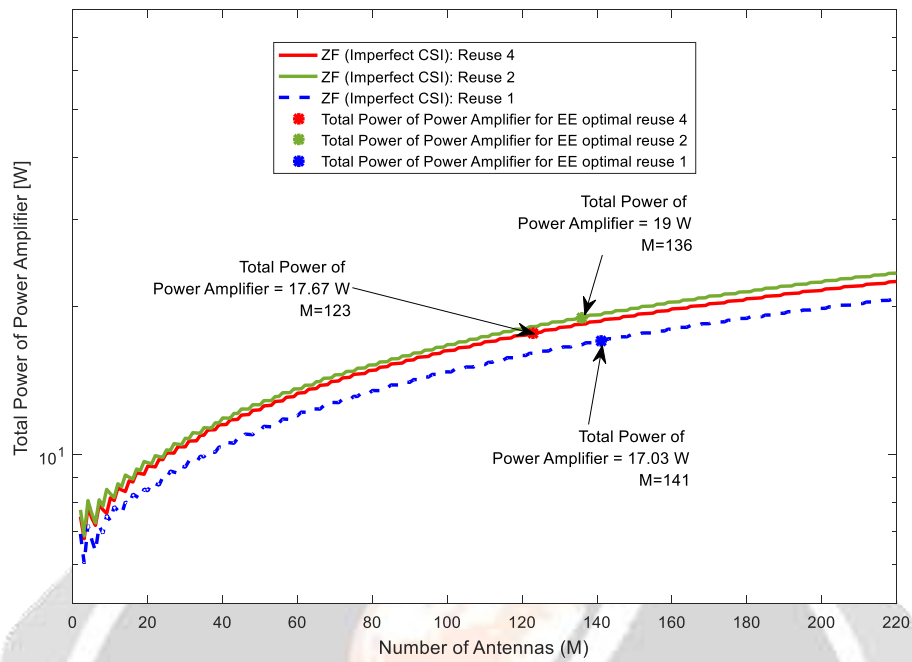


Fig -27 : Total PA powers in a large infrastructure

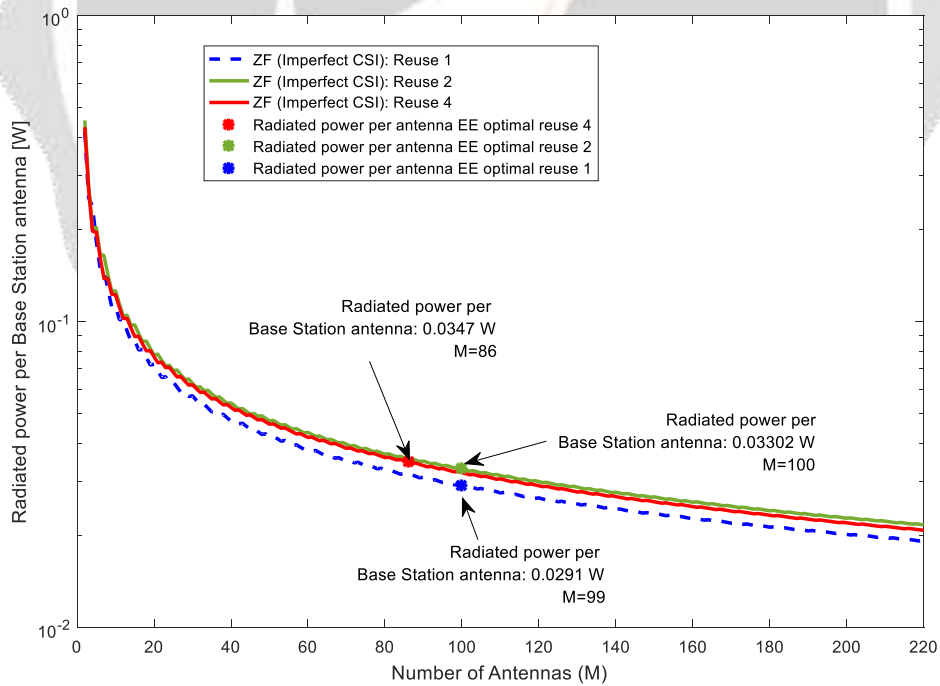


Fig -28 : Radiated Power by each antenna of the base station in dense urban space

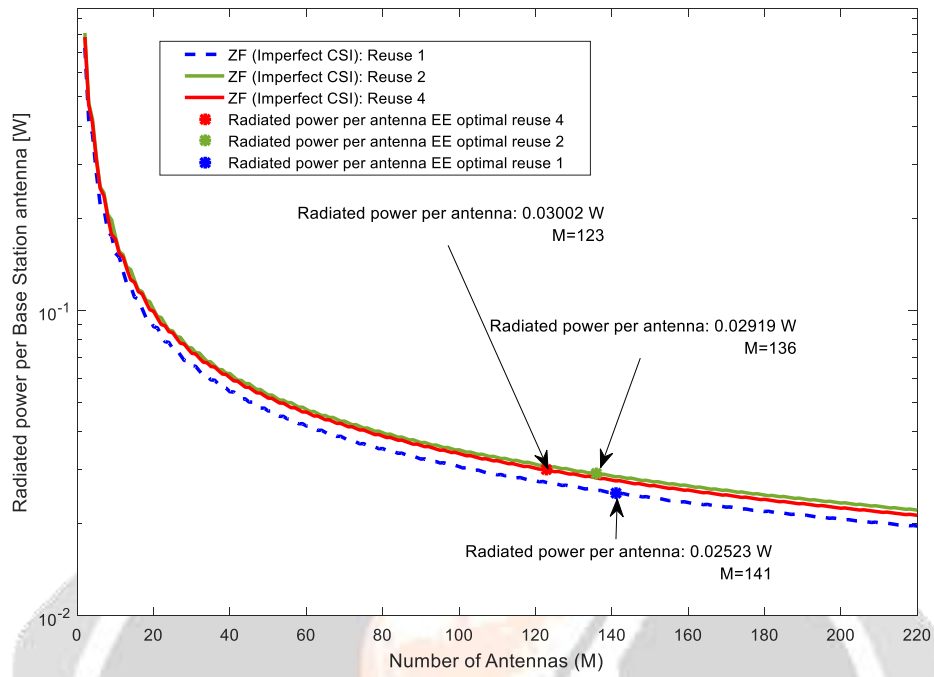


Fig -29 : Radiated Power by each antenna of the base station in a large infrastructure

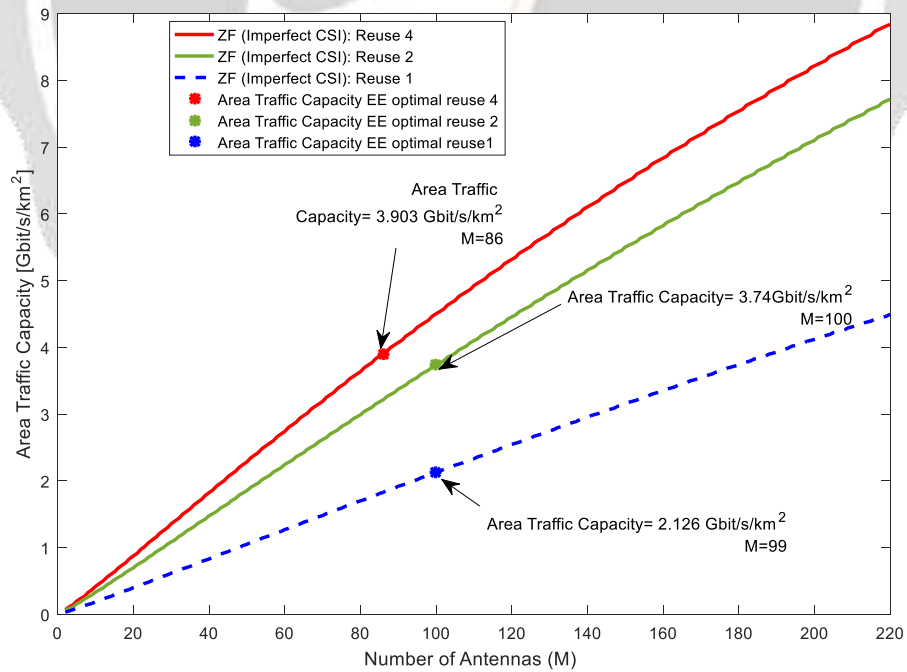


Fig -30 : Area Traffic capacity in a dense urban environment

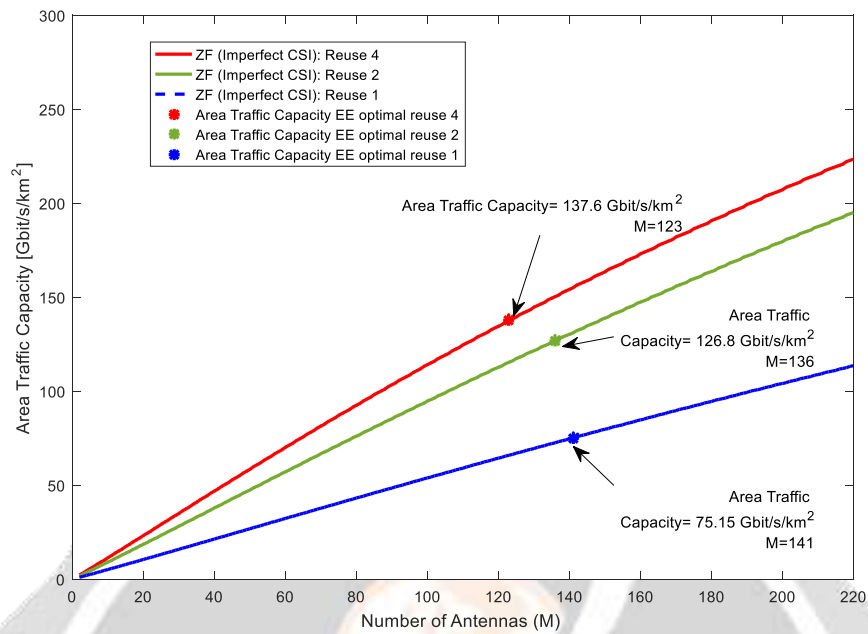


Fig -31 : Area Traffic capacity in a large infrastructure

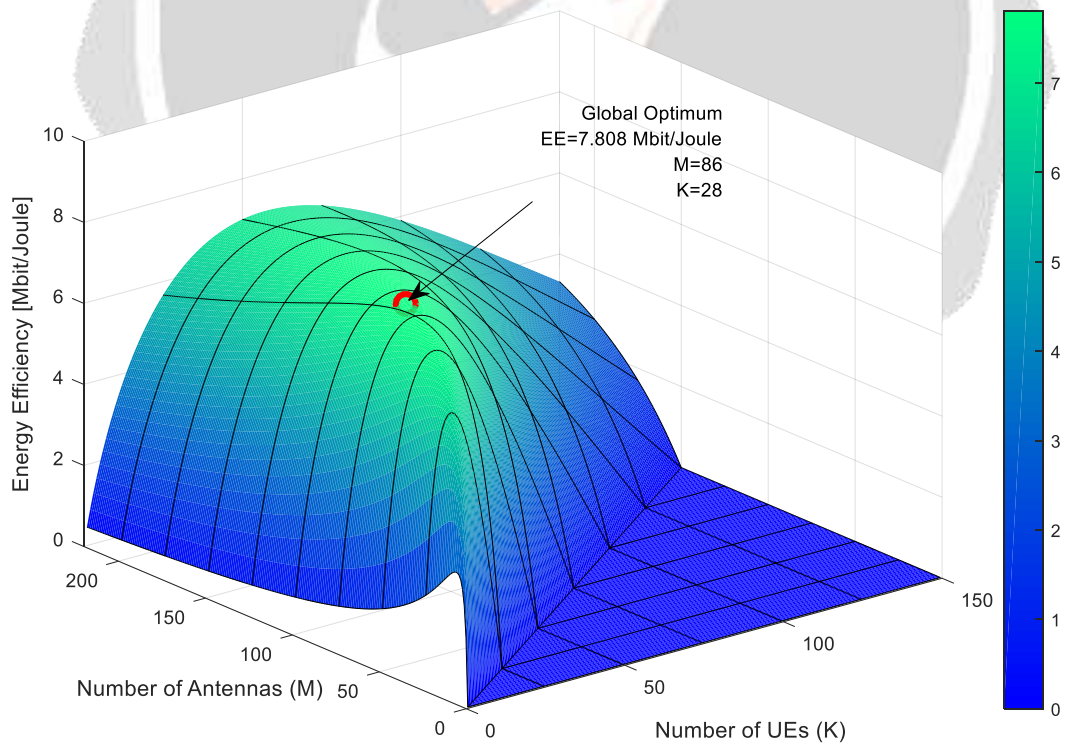


Fig -32 : Global optimum for ZF with pilot reuse 4 in multicellular scenario, in dense urban space

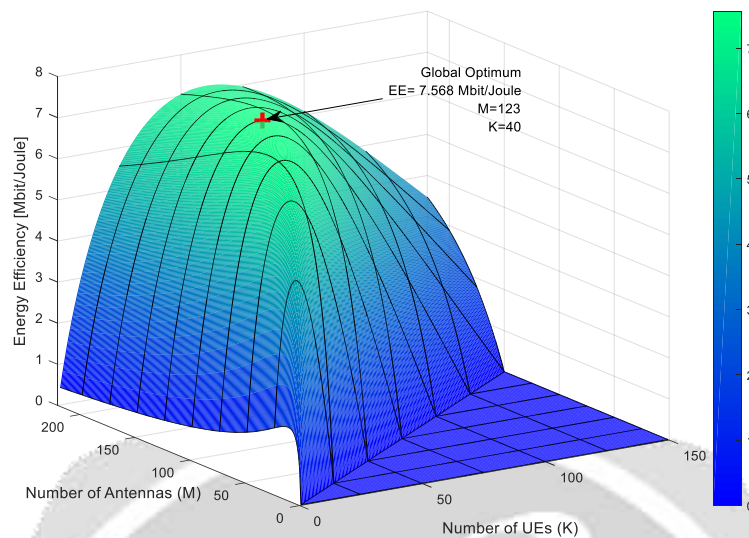


Fig -33 : Global Optimum for ZF with Pilot Reuse 4 in a Multicell Scenario, in a Large Infrastructure

3.2 Interpretations of Energy Efficiency Optimization Results in the 700 MHz Band Systems

According to the results obtained in a single-cell scenario, the ZF linear processing systems provide better Energy Efficiency and interesting traffic capacities compared to the MRT / MRC treatment system in a medium of urban space and especially in a building. Optimal EE values in dense urban space are obtained with a large number of antennas at the base station or 148 for ZF at perfect CSI, 169 for ZF at imperfect CSI and 55 for MRT / MRC at perfect CSI. That said, a Massive MIMO configuration would ensure better performance while having an energy-efficient system and high throughput for 5G telecommunications networks. The communication scenario study in a building showed us that optimal EE is always provided by a large number of antennas for ZF with very high speed up to 3414 Gbit / s / for ZF at perfect CSI but with only 54.14 Gbit / s / for MRT / MRC at perfect CSI when $M = 2$. Based on the results obtained in the multicell scenario, it is seen that the largest pilot reuse factor () gives the highest EE and the highest traffic capacity. This shows that it is necessary to actively mitigate pilot contamination in multicellular systems. However, the results of the global optimum provided in multicellular scenario give low EE compared to those provided in single-cell scenario. In a dense monocellular urban space we have: $M = 169$, $K = 98$ and $EE = 23.37$ Mbit / J against $EE = 7.808$ Mbit / J, $M = 86$ and $K = 28$. This is due to intercellular interference, which forces each cell to sacrifice certain degrees of freedom. Nevertheless, we conclude that Massive MIMO is the optimal EE architecture. In short, a ZF processing system is more desirable for systems in the 700 MHz bands with a bandwidth of 20 MHz for 5G telecommunications networks if one wants to achieve the performance requirements for these cellular networks in the single-cell scenarios. and multicellular. It is important to actively mitigate the pilot contamination for best results in a multicell scenario. Needs of new spectra are heard to guarantee more flows, hence the exploitation of higher frequencies: millimeter waves.

4 Optimization of Spectral Efficiency

Spectral Efficiency is defined as the ratio between the bit rate (in bit / s) and the bandwidth (in Hz). We have two hybrid precoding architectures. The first is the fully connected phase shifter architecture, in which each RF chain is connected to all base station antennas via phase shifters. It takes thousands of phase shifters to perform analog precoding for this architecture. Each RF channel will drive hundreds of antennas to the base station. The second architecture is phase shifted partially connected, each RF chain being connected only to a subset of base station antennas. This architecture makes it possible to reduce the number of phase shifters required. We will study these two architectures for this second part. Figure 34 and Figure 35 respectively show the block diagram of the fully connected and partially connected phase shifter hybrid precoding structure.

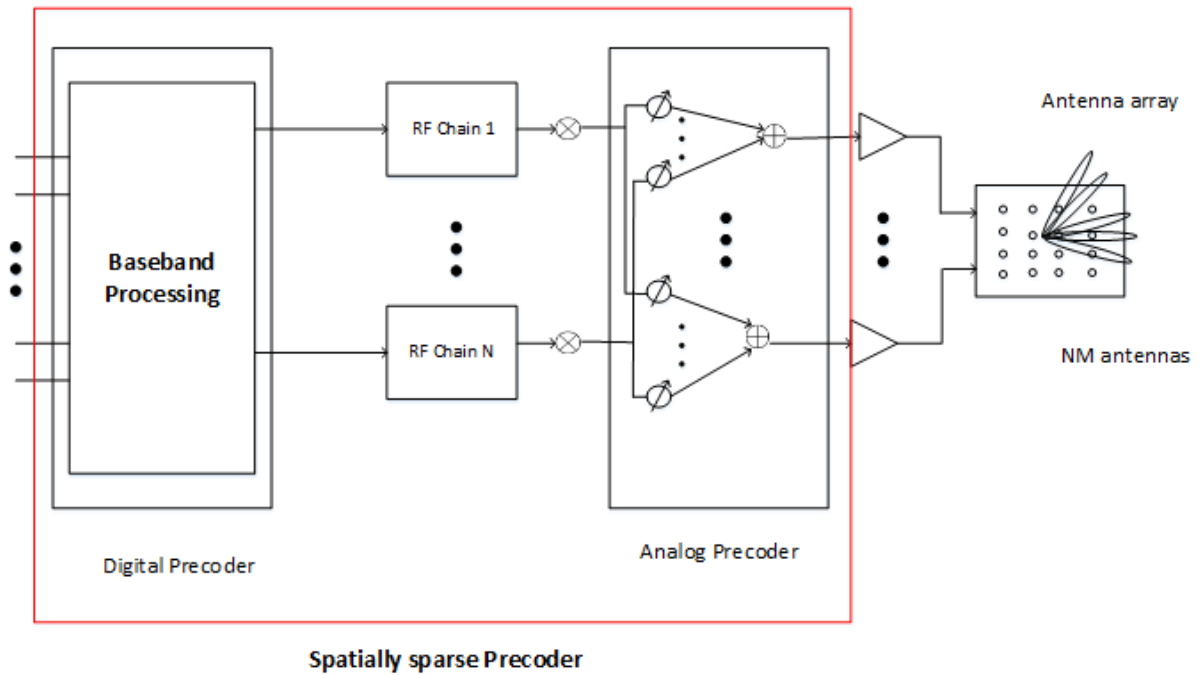


Fig -34 : Hybrid precoding structure block diagram with fully connected phase shifters in mmWave Massive MIMO system

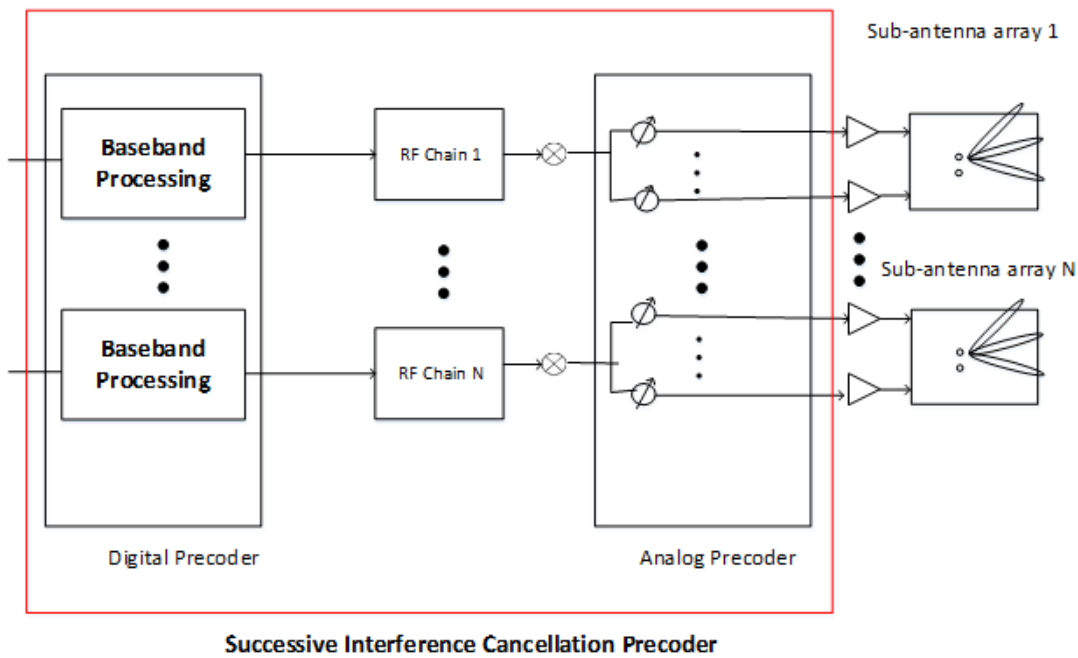


Fig -35 : Hybrid precoding structure block diagram with phase shifters partially connected in mmWave Massive MIMO system.

Two hybrid precoding optimization algorithms are discussed.

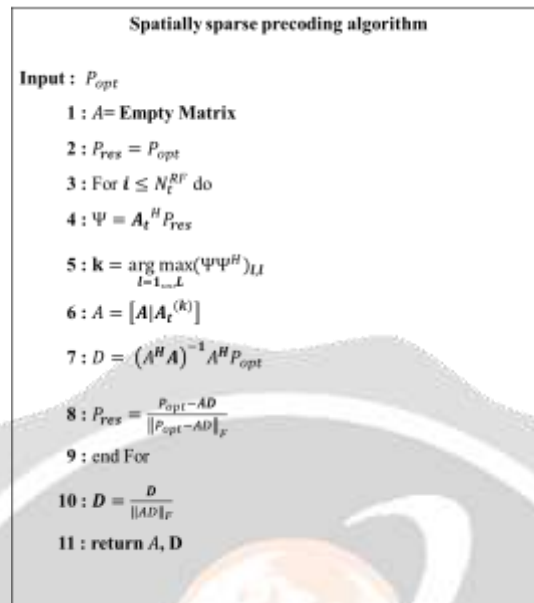


Fig -36 : Spatially sparse precoding algorithm

The spatially sparse precoding algorithm begins by finding the vector $a_t(\phi_{1,i}^t, \theta_{1,i}^t)$ according to which the optimal precoder has the maximum projection by calculating $\Psi = A_t^H P_{res}$. The index corresponding to this maximum value is calculated. It then adds the selected column vector $a_t(\phi_{1,i}^t, \theta_{1,i}^t)$ to the RF precoder A . After finding the dominant vector, we calculate the least squares solution in D step 7, the contribution of the selected vector is removed in step 8 and the algorithm searches for the column on which the residual precoding matrix P_{res} has the largest projection. The process continues until all RF beamforming vectors have been selected. At the end of N_t^{RF} iterations, the algorithm would have built an RF $N_t \times N_t^{RF}$ A precoding matrix and found the optimal $N_t^{RF} \times N_s$ baseband precoder D that minimizes $\|P_{opt} - AD\|_F^2$. Step 10 ensures that the transmit power constraint is exactly satisfied.

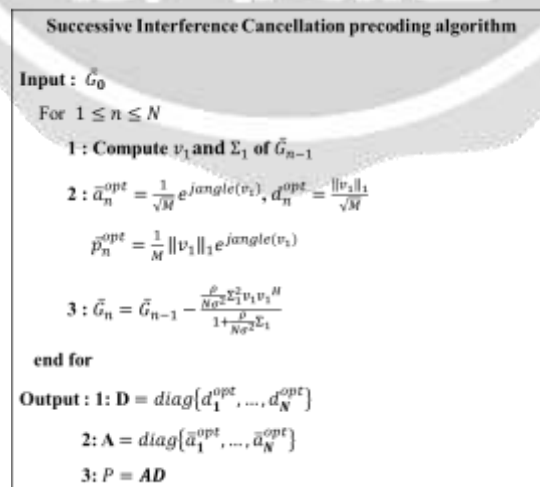


Fig -37 : Successive Interference Cancellation precoding Algorithm

The simulation parameters are described as follows. We generate the channel matrix according to the channel model like that of Saleh-Valenzuela which has been presented in [9] [10].

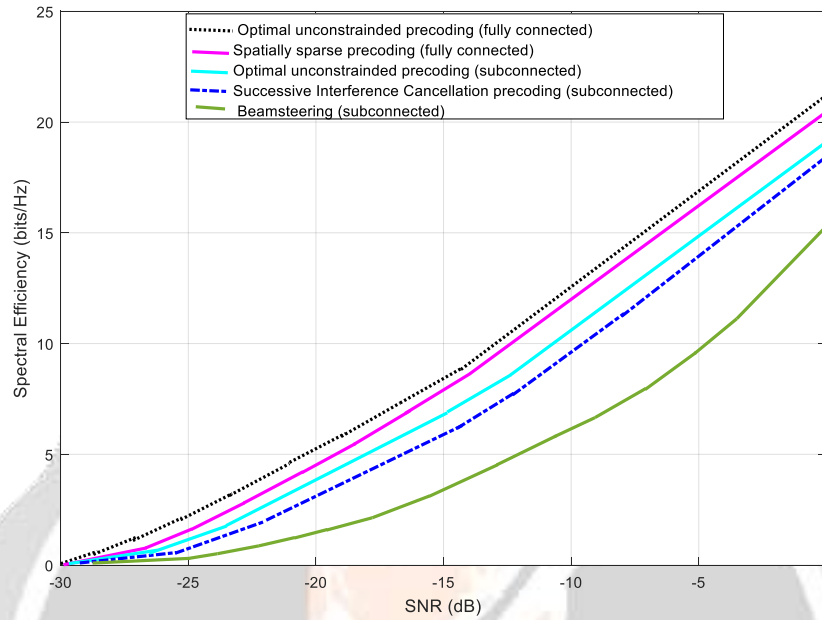


Fig -39 : Precoding comparison for mmWave massive MIMO system 64×16

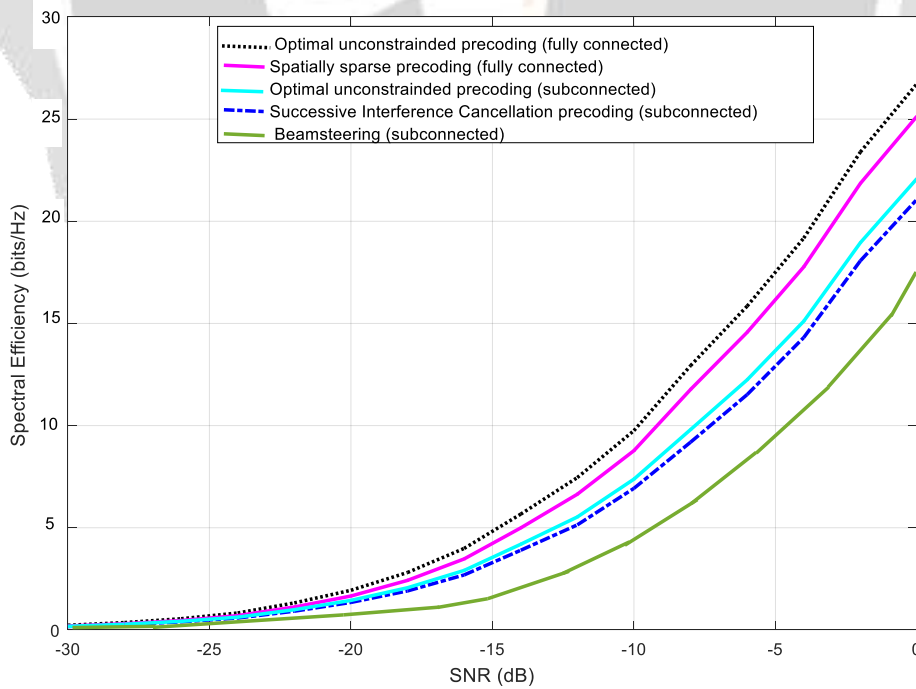


Fig -40 : Precoding comparison for mmWave massive MIMO system 128×32

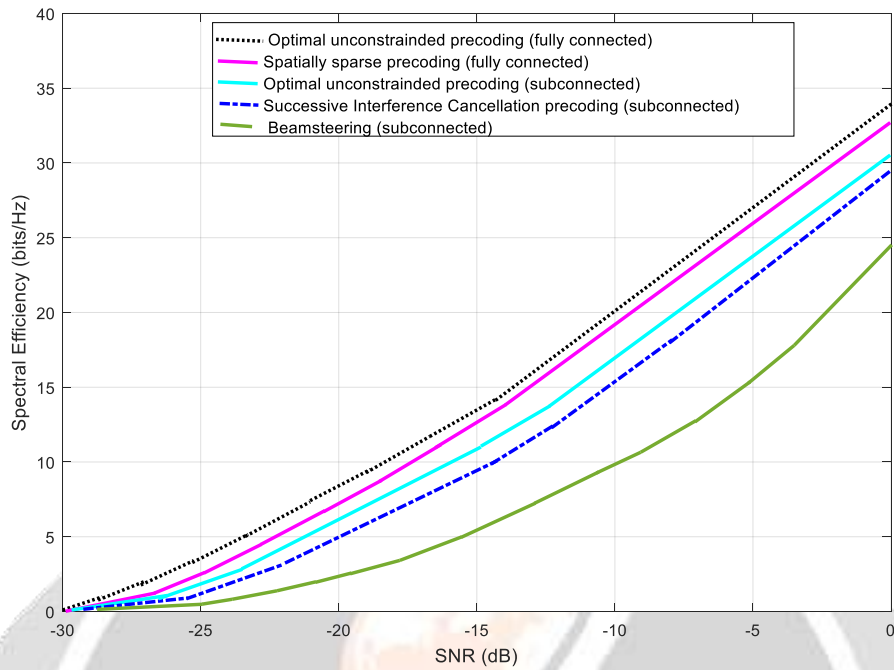


Fig -41 : Precoding comparison for mmWave massive MIMO system 256×64

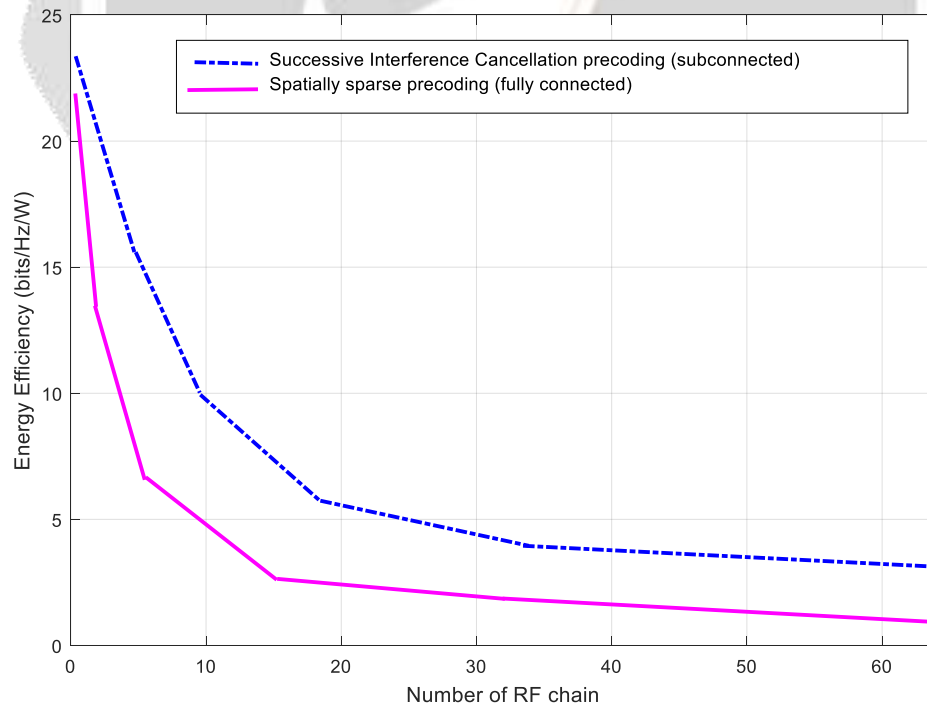


Fig -42 : Energy Efficiency 64×64

5. Conclusion

Optimization has been divided into two major parts. The first part showed simulation results of a communication scenario between base station and UE for a system using MU-MIMO using the 700 Mhz bands, with a bandwidth of 20 MHz in a single-cell and multicellular scenario in dense urban dense and in a large infrastructure. The goal is to have a system with better Energy Efficiency and maintain a high data rate also. It has been shown that Energy Efficiency can be maximized by the interaction of different key system parameters such as the number of antennas at the base station, the number of UEs and the choice of transmission power in the systems. MIMO. Wave propagation models, characteristics of the communication environment and power consumption models were considered by the different systems encompassing the network to be studied. It has been concluded that a MIMO system of about 100 antennas at the base station is of interest for maximizing the Energy Efficiency of the telecommunication network system, regardless of the study environment. The ZF treatment is better in all the simulations performed compared to the MRT / MRC treatment because of the suppression of interference by this first one. Better Energy Efficiency and better traffic capacity are noted for ZF treatment compared to MRT / MRC. In the case of a multicell system, it is necessary to actively mitigate the pilot contamination that is to say well choose the pilot reuse factor to have a good system. In the end, this first part concluded from the global optimizations obtained that Massive MIMO in the cellular networks bring improvements and can reach the challenges of energy and interesting bitrates. The second part of the optimization works on millimeter-wave systems using higher frequencies, higher frequencies from 30 GHz to 300 GHz. Still several antennas can be deployed because of the characteristics related to these frequencies for these systems even up to 200 antennas. Different precodings have been analyzed and proved that hybrid precoding systems are the best candidates for a millimeter wave system to ensure a high data rate and a more Energy Efficient system. Considering the results of comparisons between hybrid precodings, even if the Spatially Sparse fully-connected phase shifter precoding system has a slightly higher Spectral Efficiency than the partially connected Successive Interference Cancellation precoding, it is preferable to use the second, because the latter is more energy efficient.

6. REFERENCES

- [1].Y. Wu, H. Huang, C. Wang, Y. Pan, « *5G Enabled Internet Of Thing* », CRC Press,2019
- [2].E. Dahlman, S. Parvall, J. Sköld, « *5G NR : The Next Generation Wireless Access* », Academic Press, 2018.
- [3].J. MacIntyre, I. Maglogiannis, L. Iliadis, E. Pimenidis, « *Artificial Intelligence Applications and Innovations*», IFIP International Federation for Information Processing, 2019
- [4].A. Elnashar, M. El-Saidny, « *Practical Guide to LTE-A, VoLTE and IoT*», Wiley, 2018”
- [5].E. Björnson, J. Hoydis, M. Kountouris, and M. Debbah, «*Massive MIMO systems with non-ideal hardware: Energy efficiency, estimation, and capacity limits.* »IEEE Trans. Inf. Theory, vol. 60, no. 11, pp. 7112–7139, 2014.
- [6].J. Hoydis, S. ten Brink, and M. Debbah, «*Massive MIMO in the UL/DL of cellular networks: How many antennas do we need?* » IEEE J. Sel.Areas Commun., vol. 31, no. 2, pp. 160–171, 2013.
- [7].H. Ngo, E. Larsson, and T. Marzetta, «*Energy and spectral efficiency of very large multiuser MIMO systems.* » IEEE Trans. Commun., vol. 61, no. 4, pp. 1436–1449, 2013
- [8].E. Björnson, L. Sanguinetti, J. Hoydis, and M. Debbah, «*Optimal design of energy-efficient multi-user MIMO systems: Is massive MIMO the answer?* » IEEE Trans. Wireless Commun., vol. 14, no. 6, pp. 3059 – 3075, Jun. 2015
- [9] Shahid Mumtaz, Jonathan Rodriguez , Linglong Dai « *mmWave Massive MIMO :A Paradigm for 5G*», Academic Press, 2016
- [10].Xinyu Gao, Linglong Dai, Chih-Lin I, , Shuangfeng Han, Robert W. Heath Jr, «*Energy-efficient hybrid analog and digital precoding for mmWave MIMO systems with large antenna arrays*», *IEEE journal on selected areas in communications*, vol. 34, no. 4, April 2016